Marine microgels as a source of cloud condensation nuclei in the high Arctic

Mónica V. Orellana[a,1,2], Patricia A. Matrai[b,1,2], Caroline Leck[c], Carlton D. Rauschenberg[b], Allison M. Lee[a], and Esther Coz[c,d]

[a]Institute for Systems Biology, Seattle, WA 98109; [b]Bigelow Laboratory for Ocean Sciences, West Boothbay Harbor, ME 04575; [c]Department of Meteorology, Stockholm University, SE-106 91 Stockholm, Sweden; and [d]CIEMAT, Department of Environment, E-28040 Madrid, Spain

Edited* by David M. Karl, University of Hawaii, Honolulu, HI, and approved July 18, 2011 (received for review February 16, 2011)

Marine microgels play an important role in regulating ocean basin-scale biogeochemical dynamics. In this paper, we demonstrate that, in the high Arctic, marine gels with unique physicochemical characteristics originate in the organic material produced by ice algae and/or phytoplankton in the surface water. The polymers in this dissolved organic pool assembled faster and with higher microgel yields than at other latitudes. The reversible phase transitions shown by these Arctic marine gels, as a function of pH, dimethylsulfide, and dimethylsulfoniopropionate concentrations, stimulate the gels to attain sizes below 1 μm in diameter. These marine gels were identified with an antibody probe specific toward material from the surface waters, sized, and quantified in airborne aerosol, fog, and cloud water, strongly suggesting that they dominate the available cloud condensation nuclei number population in the high Arctic (north of 80°N) during the summer season. Knowledge about emergent properties of marine gels provides important new insights into the processes controlling cloud formation and radiative forcing, and links the biology at the ocean surface with cloud properties and climate over the central Arctic Ocean and, probably, all oceans.

air–sea exchange | immunological probes | *Melosira arctica*

Our limited knowledge about cloud radiative processes remains a major weakness in our understanding of the climate system and consequently in developing accurate climate projections (1). This is especially true for low-level Arctic clouds, which play a key role in regulating surface energy fluxes, affecting the freezing and melting of sea ice, when the climate is changing faster in the Arctic than at any other place on earth. The radiative or reflective (albedo) properties of clouds strongly depend on the number concentration of aerosol particles available for uptake or condensation of water vapor at a given water supersaturation. Such particles are known as cloud condensation nuclei (CCN), and their activation and growth (2) depend on the equilibrium thermodynamics by which water vapor condenses on CCN and forms a liquid cloud drop. In the high Arctic, the aerosol-cloud-radiation relationship is more complex than elsewhere, and for most of the year, the low-level clouds constitute a warming factor for climate rather than cooling (3). In summer, this is due to the semi-permanent ice cover, which raises the albedo of the surface, and to the clean Arctic air (4), which decreases the albedo of the low-level clouds. Small changes in either factor are very important to the heat transfer to the ice and the subsequent summertime ice-melt. The high Arctic CCN originate in the open leads in the pack ice and from sources along the marginal ice edge; they are formed mostly by aggregates of organic material, presumably of marine origin (5–7).

Marine polymer microgels are 3D polymer hydrogel networks that result from the spontaneous assembly/dispersion equilibrium of free biopolymers in the dissolved organic matter (DOM) pool. Microgels form hydrated Ca^{2+}-bonded supramolecular networks whose interaction with solvent (water) provides them with a gel-like texture (8–10). During the Arctic Summer Cloud Ocean Study cruise (ASCOS 08–2008, 87–88° N, 2–10° W) (Fig. S1), we characterized and quantified marine polymer gels in the subsurface waters (SSW) as well as at the air/water interface, where they concentrated, and in cloud, fog, and airborne aerosol.

Results and Discussion

We monitored the kinetics of the assembly of free polymers in the DOM pool by measuring the amount of carbon that assembled into polymer gels (see *Methods*) as a function of time (Fig. 1*A*). Our results show that polymeric material from the surface micro layer (SML) and SSW assembled spontaneously into polymer gels that ranged from colloidal to micrometer sizes, similar to polymer gels from other water sources (8, 9). The microgel concentration and size reached equilibrium at ~6–8 h (Fig. 1*A*), faster than previously reported for oceanic waters (8). Images of in situ microgels stained with chlortetracycline, obtained with confocal microscopy, show that microgels are stabilized by Ca^{2+} ionic bonds (Fig. 1*B*). Control experiments show that spontaneous assembly of microgels in the DOM is prevented when seawater Ca^{+2} and Mg^{+2} are chelated by the addition of 10 mM EDTA to the seawater; these parallel experiments demonstrate that these polymer gels are ionically bonded polymer networks (8) (Fig. 1*A*). The concentration of polymers in the DOM pool, the length of the polymer chains, and their physical chemical characteristics can affect the rate of spontaneous assembly of polymer gels (8, 9). In the Arctic Ocean, the dissolved organic carbon concentrations are high and range between 100 and 250 μM C explaining, in part, the fast rate of the assembly process. During the 21 drift days of our expedition north of 80 °N (Fig. S1), we observed an average yield of 32% (±15%; SD) of the DOM, expressed as organic carbon, assembled as microgels in either the SML or the SSW. This high percentage of assembled microgels is probably due to long-chain free polymers present in seawater (9) and corresponds to an average of 10^6 to 10^7 nanometer- (>300 nm and <1 μm) and micrometer (>1 μm)-sized polymer gels mL^{-1}, and a total of 10^{19} polymer gels mL^{-1} including the colloidal size gels (<300 nm). We also found higher yields of assembled microgels in the SSW and SML than were reported for other ocean regions [~10% (8, 10)] (Fig. 1*C*). The high abundance of polymer gels coincided with a high abundance of the diatom *Melosira arctica*, which formed large patches at the edges of the leads and are associated with high numbers of gel-forming strands several meters in length (11). Phytoplankton and marine bacteria are known to be the

Author contributions: M.V.O., P.A.M., and C.L. designed research; M.V.O., P.A.M., C.L., C.D.R., A.M.L., and E.C. performed research; M.V.O. contributed new reagents/analytic tools; M.V.O., P.A.M., and E.C. analyzed data; and M.V.O. and P.A.M. wrote the paper.

The authors declare no conflict of interest.

*This Direct Submission article had a prearranged editor.

Freely available online through the PNAS open access option.

[1]M.V.O. and P.A.M. contributed equally to this work.

[2]To whom correspondence may be addressed. E-mail: morellana@systemsbiology.org or pmatrai@bigelow.org.

This article contains supporting information online at www.pnas.org/lookup/suppl/doi:10.1073/pnas.1102457108/-/DCSupplemental.

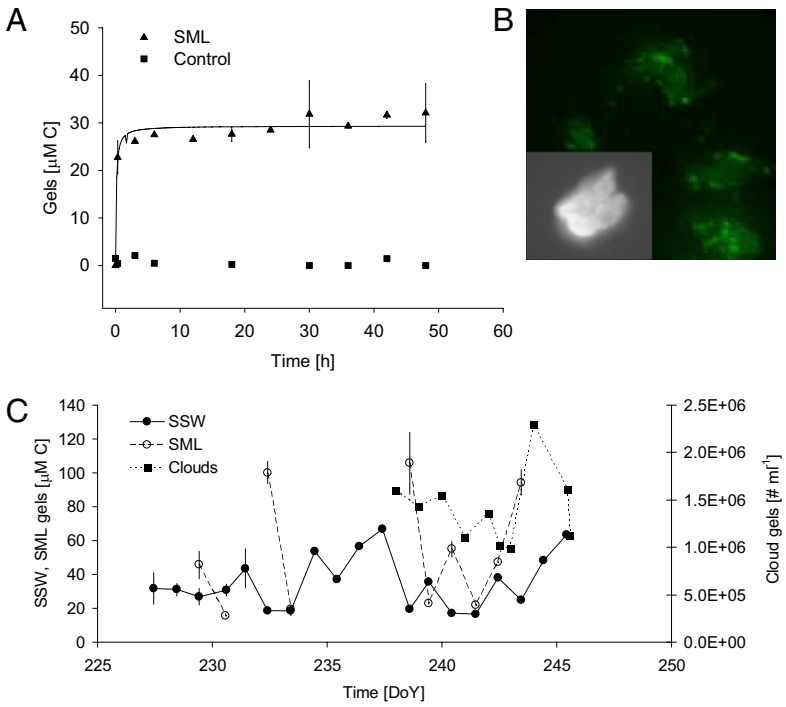

Fig. 1. Polymer gel assembly as a function of time in high Arctic surface waters. (*A*) We monitored the assembly of polymer gels by measuring the percentage of polymers assembled as microgels at 4 °C (triangles). Control experiments in which Ca^{2+} was chelated from seawater with 10 mM EDTA showed no assembled gels, regardless of the time of observation (squares). Each point corresponds to the average of three replicates. We note that the assembly occurred very quickly, with the concentration and size of assembled polymer gels reaching equilibrium in 6 h. An average yield of assembly equal to 32% of the polymers in the DOM pool was measured for either SSW or SML water samples. (*B*) Microgels. Gels stained with chlortetracycline indicate the presence of bound Ca^{2+}; insert at higher magnification. (*C*) Temporal variability in microgel concentration. During the drift phase of ASCOS at 87°N, we measured microgels in the SSW and SML in units of carbon, whereas we counted microgels in clouds with flow cytometry (as discrete particles) due to the large sample volume required to accurately measure carbon concentration in the microgels. SML microgels were enriched up to a factor of 5 with respect to SSW concentrations.

main sources of biopolymers and polymer gel networks in the oceans (12). Phytoplankton alone release ~10–50% of their primary production into the dissolved organic carbon pool in Arctic waters (13) and contain such long-chain polymers as carbohydrates (14) and proteins (15). We found these chemical compounds in the lead waters (Fig. S2). Equally important in determining an enhancement of microgel assembly kinetics by DOM polymers in the high Arctic leads is the presence of hydrophobic moieties, which have been shown to significantly increase the rate of assembly (16) and aggregation (17) and are known as important components in microgels (15). We identified hydrophobic moieties by staining the microgels with Red Nile (Fig. S3*A*), quantified proteins (Fig. S2*A*) that were frequently enriched in the SML with respect to subsurface seawater (Fig. S2*B*), and analyzed their amino acid composition (see *Methods*). We observed an enrichment of hydrophobic amino acids (leucine, isoleucine, phenylalanine, and cysteine) in the SML with respect to subsurface seawater (Fig. S3*B*), where microgel assembly probably took place (Fig. 1*A*), as well as at bubble interfaces (18), which were very abundant (19).

All polymer gels have one characteristic feature: they undergo reversible volume phase transition, changing from a swollen and hydrated phase to a condensed and collapsed phase and back, in association with the internal dielectric properties of the gel polymer matrix (20). Because of the relevance in high latitudes of ubiquitous and important climate chemical compounds such as dimethyl sulfide (DMS) and its oxidation product sulfuric acid (H_2SO_4), we demonstrate that these chemicals induced reversible volume phase transitions in the microgels (Fig. 2 *A* and *B*). A steep volume transition from hydrated phase to condensed phase takes place as the pH is decreased from pH 8 to 6. This transition pH is higher than previously observed (pH 4) for marine polymer gels from other latitudes (8). Although the low transition pH measured by Chin et al. (8) is not yet a relevant value in today's ocean [pH 8.05 (21)], the rationale for the experimental use of H_2SO_4 in this study was based on the fact that H_2SO_4 is a product of the atmospheric oxidation of DMS in the marine boundary layer (4, 22) and has been shown to be relevant to the growth of new nanometer-size atmospheric particles (23) over the pack ice area. The condensation and volume collapse of these ionic polymeric networks were also caused by additions of nano- to micromolar levels of DMS and its biogenic precursor dimethylsulfoniopropionate (DMSP) (Fig. 2*B*), that are in agreement with high extracellular and intracellular concentrations of these important climate chemical compounds produced by polar phytoplankton and ice algae (24). These results are analogous to the finding that high concentrations of DMSP and DMS are stored in the acidic secretory vesicles of the microalga *Phaeocystis antarctica* where DMSP is trapped within the condensed polyanionic gel matrix (25) until the secretory vesicles are triggered by environmental factors to release microgels that undergo volume phase transition and expand at the higher pH of seawater (26). Exocytosis of polymer gels accompanied by elevated DMS and DMSP concentrations suggests the transport of these chemical compounds by the gel matrix (25).

In addition to the occurrence of microgels in seawater, we demonstrate here the presence of marine polymer microgels in cloud, fog, and airborne aerosol particles sampled at 87°N (Fig. 3*A* and S4 *A* and *B*). Cloud microgels reacted positively with an antibody specific toward material from the surface waters, indicating that the source of the gel particles detected in clouds was

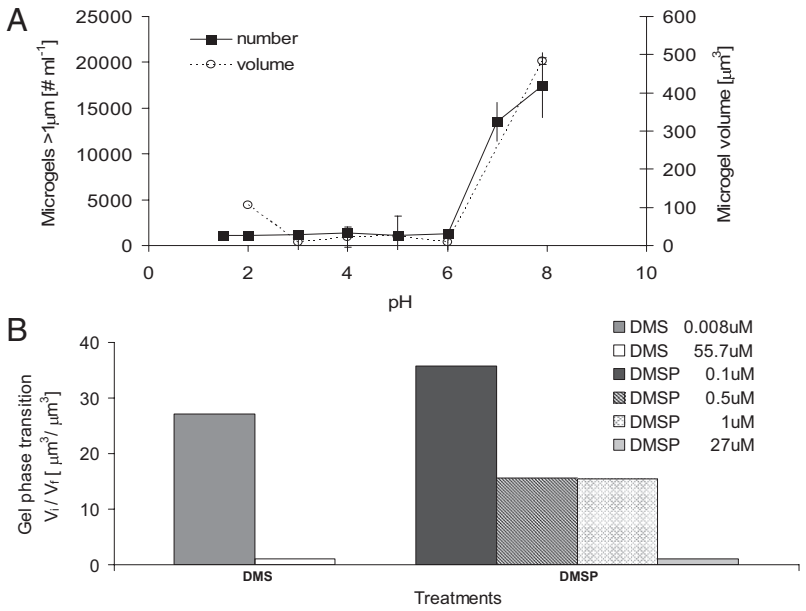

Fig. 2. Microgel volume phase transition. (*A*) pH. Marine polymer gels can undergo a fast reversible volume phase transition (<1 min) from a swollen or hydrated phase to a condensed and collapsed phase by changing the pH of the sea water with H_2SO_4. We then stained the polymer gels with chlortetracycline, monitored the size of the polymer gels by confocal microscopy, and monitored the number of gels by flow cytometry. The swelling/condensation transition is reversible and has a steep sigmoidal change in the volume of the gels. Each data point corresponds to the average and SD of three samples. (*B*) DMS and DMSP. Marine polymer gels can undergo a fast, reversible change from a swelled/hydrated phase to a condensed phase as a function of DMS and DMSP concentrations, expressed as the ratio between initial (Vi) and final (Vf) microgel volume before and after adding the inducing compound, respectively, and measured with confocal microscopy.

the surface water and, most probably, the SML where microgels accumulated. Similar antibody results were found for the particles in the fog and aerosols (Fig. S4 *A* and *B*). This polymeric material could have come from phytoplankton, such as *M. arctica* and their exocytosed products, because this species cross-reacted with the antibody from the surface water DOM (microscopic observation/antibody cross reactivity, Table S1). Polymer microgels reached 2.00 ± 0.96 mg (dry weight) L^{-1} of cloud water (these results do not include material smaller than 0.2 µm in diameter), as determined by a specific ELISA (see *Methods*). The size distribution of all microgels in their native state, as well as those immunostained with the antibody probe in the cloud, fog, and low altitude airborne aerosol samples, follows an expected pattern with higher numbers in the very small sizes. More than 80% of the particles were smaller than 100 nm in diameter, and nearly 100% were smaller than 200 nm (Fig. 3*B*, 1 and 2), corresponding to $2–8{\cdot}10^{11}$ nanometer-sized gels mL^{-1} and $2{\cdot}10^{9}$ µm-sized gels mL^{-1} of cloud water. The morphology and structure of the microgels, as independently examined by field emission scanning electron microscopy (FESEM) of unstained samples and confocal microscopy of immunostained samples (see *Methods*), were very consistent, showing high numbers of nanometer-sized gels (Fig. 3*C*, 3 and 4). While the higher sensitivity and resolution of the FESEM allowed the quantification of native gels as small as 2 nm in diameter, the resolution of the confocal microscope used to analyze the immunostained gels was slightly lower (20 nm) (Fig. 3*B*, 1 and 2). This analytical difference resulted in higher immunostained particle counts in the larger size ranges (Fig. 3*B*, 2), but we observed an identical modal appearance when we set the FESEM resolution to match the confocal setting (Fig. 3*B*, 1). The similarity in size distribution of both immuno-stained and total particle populations suggests that the particles present experienced similar atmospheric processing, not only in the cloud and fog but also in the aerosol (Fig. S4 *C* and *D*), with implications not only for cloud formation but also for providing the source of the newly formed particles (27). Both approaches showed that nanometer-sized gels tend to present a fractal structure (Fig. 3*C*, 2) (28), with a diffuse organic surface (Fig. 3*C*, 5); indeed, observations of the micromolar-sized particles at higher magnification showed tangled nanometer-sized gels that annealed to form the larger micromolar-sized gels (Fig. 3*C*, 2 and 3).

Whereas organic particles have been shown to be present in clouds (29), the unique physicochemical characteristics of marine microgels in clouds, such as their ability to undergo volume phase transition in response to environmental stimuli (pH, temperature, chemical compounds, and pollutants) and the cleavage of their polymers by UV radiation (9), have not been previously shown. The emergent properties of airborne gels can affect the chemistry and physics of the Earth's atmosphere by being a source of CCN in the Arctic and, most likely, elsewhere (6), because source marine microgels are present in the seawater DOM of all oceans. The very gel nature of these marine particles defines them as hydrated and hygroscopic, which, tied to the very low CCN numbers observed (30) and the very high relative humidity over the remote pack ice area in summer, strongly suggests that the cloud microgels are CCN. Previous evidence (5, 31) suggests a contribution to the Aitken mode population (25–80 nm in diameter) of aerosol particles from the separation of components, or building blocks, of larger airborne colloidal gels. As previously demonstrated (9), UV radiation can easily break and cleave abundant colloidal-size gels in the ocean surface (>300 to <700 nm) into smaller nanometer-sized polymeric chains (nanogels) (Fig. S5). This mechanism is possibly active in evaporating cloud or fog and aerosol gels as well, where gel fragmentation could potentially produce millions of still smaller particles, ranging from ~40 nm down to a few nanometers in diameter (27), thus influencing new particle formation, increasing the CCN number concentration (32) and affecting cloud optical properties. Our field in situ experiments also show that polymer microgels and free polymers from the SML irradiated for 8 h at ambient fluxes of UV-B cleaved the polymers from micrometer sizes to sizes below the limit of detection of our flow cytometer (300–500 nm).

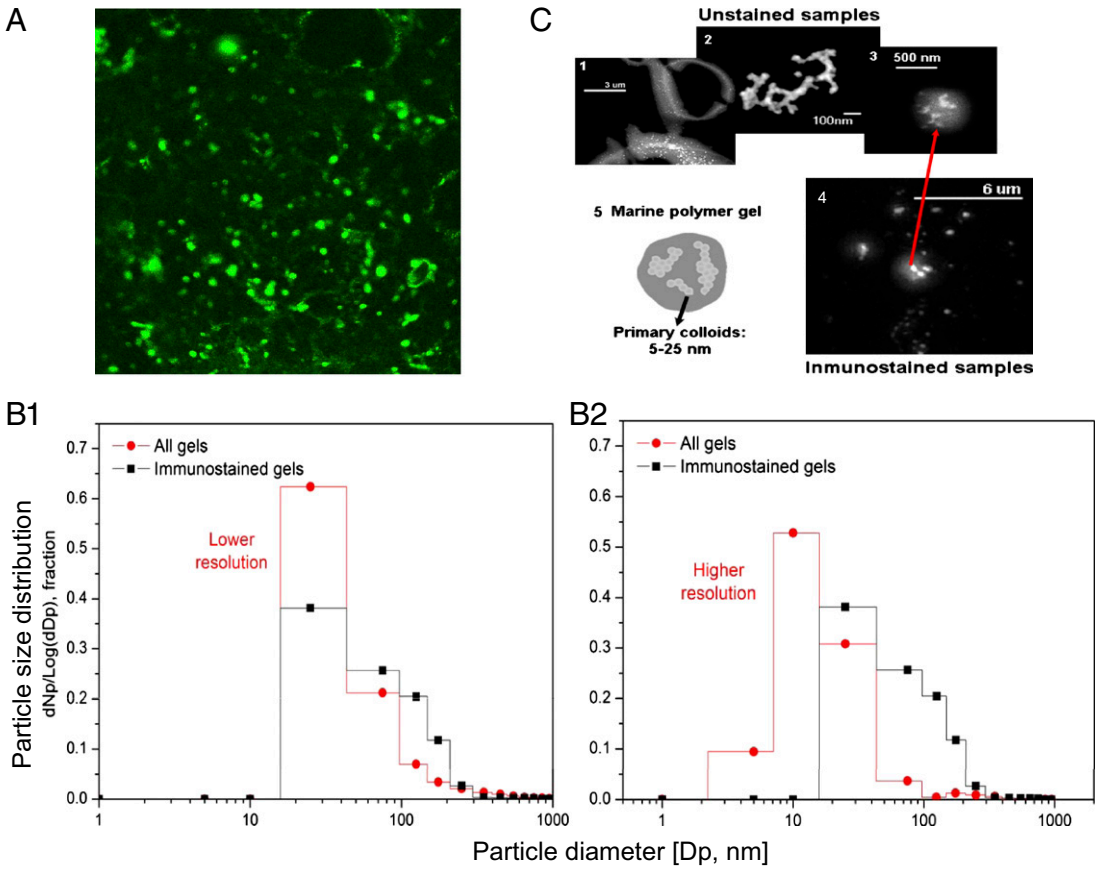

Fig. 3. Microgels in clouds. (*A*) Immunostained gels. Nanometer (nanogels)- and micrometer (microgels)-sized polymer gels immunostained with a specific antibody developed toward polymeric material collected in SML and SSW. (*B*) Gel size distribution from two independently analyzed subsamples. *B*1, Relative frequency of particle number (Np) [dNp/log(dDp): delta of Np/log delta particle diameter (Dp)] in a specific size range for unstained nanogels observed with FESEM (circles) and immunostained gels observed with confocal microscopy (squares), with instruments held at a similar, lower resolution. *B*2, The higher resolution of the FESEM allows the measurement of nanogels smaller than 10 nm. (*C*) Structure of nano and microgels. (*C*1) Low water-soluble organic particles in the SML present large quantities of colloidal-sized nanogels (<1 μm), which annealed into microgels bigger than 3 μm. (*C*2) Colloidal-sized nanogels tend to present fractal structures in sizes generally <200 nm and always smaller than 1 μm in both SML and cloud samples. (*C*3 and *C*4) The gels in the cloud samples present average sizes between 200 and 700 nm, with nanogels partitioned inside of both nonstained and immunostained particles. (*C*5) The schematic illustration shows that colloidal-sized nanogels tend to present a fractal structure, with a diffuse organic surface.

In addition, the yields of microgel assembly declined significantly from 26.7 ± 5% to 8.8 ± 0.4% (SD), as expected for shorter size polymers (9). Dispersion of polymer gels and fragmentation of biopolymers, as previously demonstrated (9), could be accelerated in the clouds, where UV radiation fluxes are higher (33). We speculate that cloud microgels could also undergo reversible volume phase transitions from swollen/hydrated to condensed smaller sized microgel particles due to UV radiation (34), a change in pH (in situ cloud water pH ≤ 5.6), high DMS concentrations (4), and/or temperature (20). Indeed, the size distribution of the building blocks of airborne aggregates (5) reportedly shifted to smaller nanometer gel sizes (40-nm diameter mode; similar to our observed size distribution, shown in Fig. 3) with respect to the micron size distribution observed in water aggregates, probably due to a combination of all such environmental controls present in regions of the high Arctic where these putative microgels represented most of the sampled aerosol particles.

Bubble bursting and particle ejection processes are thought to be the likely source of the cloud and fog microgels herein described, most likely local, although an upwind ice edge location from the ocean surface into the atmosphere is not precluded (Fig. S1*C*) (6). Before bursting, bubbles rest on the SML, which is enriched in organic material in Arctic waters (35) and elsewhere; thus, the bubble films are largely comprise of polymers (18) that can assemble into microgels, if they are not already assembled, especially because of high Ca^{2+} levels favorable to ionic polymer assembly (8). The bubble-size spectra observed in high Arctic leads were comparable to those observed elsewhere, although with more abundant, smaller-sized bubbles (19), despite the lack of sea spray (absence of wave breaking) due to the presence of low winds ($U < 6\ ms^{-1}$) and short open-water fetch caused by the pack ice. On the other hand, recent direct eddy covariance measurements of particle number fluxes from the same location (36) suggest that horizontal transport from the open water near the marginal ice zone, new particle formation, and chemical transformations may also affect the particle number concentration. Notwithstanding their physical sea-to-air transfer mechanism, marine biogenic microgels were specifically identified and quantified in clouds, fogs, and airborne aerosol particles in the marine boundary layer over our study site north of 80 °N.

Our results clearly demonstrate that marine hydrogels, due to their unique physicochemical properties, can affect the chemistry and physics of the Earth's atmosphere by serving as an important source of CCN in the pristine high Arctic summer and probably elsewhere, thus affecting climate by increased warming and radiative coupling. The microgel-climate feedback paradigm suggests that biology plays an important role in determining the chemistry and physics of marine aerosol particles, such that parameteriza-

tions of their source function should include processes pertaining to the source and concentration of marine organic matter and should be included in regional and global aerosol climate models.

Materials and Methods

Sampling. We obtained samples during the drift phase (13 August to 1 September 2008) of the international ASCOS (www.ascos.se) field campaign to the high Arctic Ocean (Fig. S1 *A* and *B*). We used 5-d, 3D air mass trajectories, with an arrival height of 100 m, at the position of the icebreaker (Fig. S1*C*). We calculated the 3D trajectories from the reanalysis data library by using the HY-brid Single-Particle Lagrangian Integrated Trajectory (HYSPLIT4) model (37, 38). The data originated from the National Weather Service's National Centers for Environmental Prediction's Global Data Assimilation System. The wind fields and air mass trajectories showed that the sampled area, north of 80°N, during the drift was within air with a minimal influence by anthropogenic pollution. Direct contamination from the ship was excluded by using a pollution controller (39). We performed all water sampling ~1.5 km away from the ship. We obtained SML samples with battery-operated catamaran-type vessels fitted with a rotating drum covered with a thin sheet of sodium-in-liquid-ammonia-edged (hydrophilic) Teflon film (35). The depth of the SML sampled ranged from 2 to 41 μm. We performed SSW sampling with acid-cleaned bottles rinsed in distilled deionized water (18 MΩ) at <30 cm below the SML. We collected cloud water by deploying polypropylene filaments [acid-cleaned and rinsed with distilled deionized water (18 MΩ)] in the clouds for several (3–4) hours with a tethered balloon (40). The cloud liquid water content peaked at ~0.2 g m^{-3}. We collected fog and aerosol particles as described (41–43). We deployed a cascade impactor, which used two jet impaction stages with cut diameters at 6 and 40 μm aerodynamic diameter to collect liquid fog water samples. The nominal volumetric flow rate was 500 m^3 h^{-1} (44).

Microgel Measurements. Marine microgels are defined by a set of three physical properties that allow their examination and categorization: all marine microgels undergo phase transition; marine microgels stain with chlortetracycline (CTC, 50 μM, pH 8.0), because their polymers are stabilized by Ca^{2+} ionic bonds; and microgels disperse following calcium chelation by 10 mM EDTA (pH 8) (8, 9, 15). Samples stained with chlortetracycline (λex = 374 nm, λem = 560 nm) were observed in the field with an Olympus microscope with epifluorescence and phase-contrast, as well as documented, quantified, and measured with a Diagnostic Instruments CoolSnapES2 4 Meg slider DDC digital camera and Nikon NIS Elements software. Gels were also quantified fluorometrically (45) with pH measured spectrophotometrically (46). Microgels, ≥300 nm in size, were counted with an InFlux (Cytopeia, Inc.) flow-sorter. Immunostained cloud microgels were only documented with a Delta Vision confocal microscope, whereas parallel samples of nonstained cloud microgels and low water soluble particles were independently documented with a FESEM. We counted and sized all cloud, fog, and aerosol particles with Aphelion software. Whenever volume was available, we subsampled aerosol, cloud, and fog collections for independent FESEM and immunostaining-confocal analyses; this assumed each original sample to be fully mixed. We also identified particles by morphology and chemistry (47). We analyzed proteins (size fraction ≥ 0.7 μm) (48) and amino acids (size fractions 0.2–0.7 μm and ≤0.2 μm) (49).

Immunostaining. An antibody probe against concentrated microgels and other dissolved organic material in the SML and SSW was prepared at the Institute for Systems Biology and developed in rabbits by ABMAX AntibodyChina.com. The specificity of the antibody was analyzed by cross-reactivity against 40 different taxa of phytoplankton species, phytoplankton collected from Puget Sound, and *M. arctica* from ASCOS (Table S1) and detected by immunofluorescence coupled with flow cytometry, which indicated a high specificity toward the arctic polymeric material. An indirect ELISA was developed for arctic microgels (50) by using an antibody probe developed against polymeric material present in the SML and SSW and a secondary goat anti-rabbit biotin-conjugated antibody (Pierce 31807). The antibody was detected with a poly-HRP streptavidin and a fluorogenic peroxidase substrate solution (Pierce 15169), measured at 420 nm. The assay was optimized for antigen and antibody concentrations and for incubation length by checkerboard titration to give a maximal signal range. A calibration curve with three replicates with dry, lyophilized microgel material was included in each plate.

Polymer Gel Assembly. We monitored the polymer gel assembly by measuring carbon bound into assembled microgels (45). Triplicate seawater samples were gravity filtered immediately after sampling with Whatman GF/F glass fiber filters and a 0.22-μm Millipore filter (prewashed with 0.1N HCL) onto black bottles and then allowed to assemble over time. We monitored polymer assembly for 5 d at 4 °C and measured fluorescently labeled microgels in 7-mL cuvettes in a Turner AU-10 fluorometer. In parallel control experiments, we inhibited the assembly by chelating Ca^{+2}, Mg^{+2}, and other metals by adding 10 mM EDTA to the seawater; in addition, assembly was run in triplicate samples containing 0.02% sodium azide to prevent all microbiological contamination. We repeated these experiments on five occasions with similar results.

Polymer Gel Reversible Volume Phase Transition. Swelling/condensation transition was performed at 4 °C by monitoring changes in volume of the microgels in seawater at different pH (from 7.9 to 2) induced by increasing concentrations of H_2SO_4. Changes in volume were recorded by flow cytometer measurements of microgel forward scatter and/or by microphotographic measurements. In the case of the experiments counted with flow cytometry, microgels may undergo volume phase transition to sizes below the limit of detection of the instrument, but as soon as the pH is increased, the microgels can be recounted. We also measured volume phase transition of microgels in sea water in the presence of DMS and DMSP (10^{-3} to 10^{-9} M solutions).

Chemical Characterization. We determined the concentrations of amino acids (49, 51), carbohydrates (52, 53), dimethyl sulfide and DMSP (54), lipids (55), proteins (48, 56), and total organic carbon (57).

ACKNOWLEDGMENTS. We thank A.J. Hind, Q. Gao, C. Birch, I. Brooks, J. Knulst, T. Mauritsen, A. Sirevaag, and S. de la Rosa for invaluable help in field sampling; J. Paatero for UV data; and A. Armstrong and D. Rodriguez for technical support. ASCOS would not have been possible without the organization and support of M. Tjernström. Sampling would not have been possible without the logistical support of and/or bear-guarding by the rest of the scientific party, the Icebreaker Oden's Captain Mattias Peterson and crew, and the staff of the Swedish Polar Research Secretariat. We thank N.S. Baliga and Institute for Systems Biology for providing a stimulating environment and several anonymous reviewers for their constructive comments. M.V.O, P.A.M., C.D.R., and A.M.L were supported by grants from the US National Science Foundation, Arctic Natural Sciences program ARC-0707555 (M.V.O.), and ARC- 0707513 (P.A.M.). C.L. and E.C. were supported by the Swedish Natural Research Council. The framework of ASCOS was supported by the Swedish Research Council, the Knut and Alice Wallenberg Foundation, Developing Arctic Modeling and Observing Capabilities for Long-term Environmental Studies (European Union 6th Framework Program), and the Natural Environmental Research Council.

1. Solomon S, et al. (2007) Climate change 2007: The physical science basis, contribution of working group 1 to the fourth assessment report of the Intergovernmental Panel on Climate Change. *Intergovernmental Panel on Climate Change*, eds Solomon S, et al. (Cambridge University Press, New York, NY), p 996.
2. Koåhler H (1936) The nucleus in and the growth of hygroscopic droplets. *Trans Faraday Soc* 32:1152–1161.
3. Intrieri J, et al. (2002) An annual cycle of Arctic surface cloud forcing at SHEBA. *J Geophys Res Oceans*, 107:10.1029/2000JC000439.
4. Leck C, Persson C (1996) Seasonal and short-term variability in dimethyl sulfide, sulfur dioxide and biogenic sulfur and sea salt aerosol particles in the arctic marine boundary layer during summer and autumn. *Tellus* 48B:272–299.
5. Leck C, Bigg K (2005) Biogenic particles in the surface microlayer and overlaying atmosphere in the central Arctic Ocean during summer. *Tellus* 57B:305–316.
6. Bigg EK, Leck C (2008) The composition of fragments of bubbles bursting at the ocean surface. *J Geophys Res Atmospheres*, 113:10.1029/2007JD009078.
7. Bigg E, Leck C (2001) Cloud-active particles over the central Arctic Ocean. *J Geophys Res Atmospheres* 106:32155–32166.
8. Chin W-C, Orellana MV, Verdugo P (1998) Spontaneous assembly of marine dissolved organic matter into polymer gels. *Nature* 391:568–572.
9. Orellana MV, Verdugo P (2003) Ultaviolet radiation blocks the organic carbon exchange between the dissolved phase and the gel phase in the ocean. *Limnol Oceanogr* 48:1618–1623.
10. Verdugo P, et al. (2004) The oceanic gel phase: a bridge in the DOM-POM continuum. *Mar Chem* 92:67–85.
11. Melnikov IA (1997) *The Arctic sea ice ecosystem* (Gordon and Breach Science Publications, Amsterdam).
12. Aluwihare LI, Repeta DJ, Chen RF (1997) A major biopolymeric component to dissolved organic carbon in surface sea water. *Nature* 387:166–169.
13. Vernet M, Matrai PA, Andreassen I (1998) Synthesis of particulate and extracellular carbon by phytoplankton at the marginal ice zone in the Barents Sea. *J Geophys Res Oceans* 103:1023–1037.
14. Biddanda B, Benner R (1997) Carbon, nitrogen, and carbohydrate fluxes during the production of particulate and dissolved organic matter by marine phytoplankton. *Limnol Oceanogr* 42:506–518.

15. Orellana MV, et al. (2007) Marine microgels: Optical and proteomic fingerprints. *Mar Chem* 105:229–239.
16. Ding Y-X, et al. (2008) Amphiphilic exopolymers from *Sagittula stellata* induce DOM self-assembly and formation of marine microgels. *Mar Chem* 112:11–19.
17. Maitra U, Mukhopadhyay S, Sarkar A, Rao P, Indi SS (2001) Hydrophobic pockets in a nonpolymeric aqueous gel: observation of such a gelation process by color change. *Angew Chem Int Ed Engl* 40:2281–2283.
18. Zhou J, Mopper K, Passow U (1998) The role of surface-active carbohydrates in the formation of transparent exopolymer particles by bubble adsorption of seawater. *Limnol Oceanogr* 43:1860–1871.
19. Norris SJ, et al. (2011) Measurements of bubble size spectra within leads in the Arctic summer pack ice. *Ocean Science* 7:129–139.
20. Tanaka T, et al. (1980) Phase transitions in ionic gels. *Phys Rev Lett* 45:1636–1639.
21. Feely RA, Doney SC, Cooley SR (2009) Ocean acidification: Present conditions and future changes in a high-CO_2 world. *Oceanography (Wash DC)* 22:36–47.
22. Leck C, Bigg EK (2007) A modified aerosol-cloud-climate feedback hypothesis. *Environ Chem* 4:400–403.
23. Leck C, Bigg EK (2005) Source and evolution of the marine aerosol: A new perspective. *Geophys Res Lett*, 32:10.1029/2005GL023651.
24. Matrai PA, Vernet M (1997) Dynamics of the vernal bloom in the marginal ice zone of the Barents Sea: Dimethyl sulfide and dimethylsulfoniopropionate budgets. *J Geophys Res Oceans* 102:22965–22979.
25. Orellana MV, Matrai PA, Janer M, Rauschenberg C (2011) DMSP storage in *Phaeocystis* secretory vesicles. *J Phycol* 47:112–117.
26. Chin W-C, Orellana MV, Quesada I, Verdugo P (2004) Secretion in unicellular marine phytoplankton: demonstration of regulated exocytosis in *Phaeocystis globosa*. *Plant Cell Physiol* 45:535–542.
27. Leck C, Bigg EK (2010) New particle formation of marine biological origin. *Aerosol Sci Technol* 44:570–577.
28. Lua R, Borovinskiy AL, Grosberg AY (2004) Fractal and statistical properties of large compact polymers: a computational study. *Polym Bull* 45:717–731.
29. Herckes P, et al. (2002) The organic composition of radiation fog in Davis (California). *Atmos Res* 64:99–108.
30. Mauritsen T, et al. (2011) An Arctic CCN-limited cloud-aerosol regime. *Atmos Chem Phys* 11:165–173.
31. Leck C, Bigg E (1999) Aerosol production over remote marine areas: A new route. *Geophys Res Lett* 23:3577–3581.
32. Lohmann U, Leck C (2005) Importance of submicron surface active organic aerosols for pristine Arctic clouds. *Tellus* 57B:261–268.
33. International-Arctic-Science-Committee (2010) Long-term change and variability in surface UV irradiance in the Arctic. *Encyclopedia of Earth*, eds Cleveland CJ, et al. (Environmental Information Coalition, National Council for Science and the Environment, Washington, DC).
34. Mamada A, Tanaka T, Kungwatchakun D, Irie M (1990) Photoinduced phase transition of gels. *Macromolecules* 23:1517–1519.
35. Matrai PA, Tranvik L, Leck C, Knulst J (2008) Are high Arctic microlayers a potential source of aerosol organic precursors? *Mar Chem* 108:109–122.
36. Held A, Brooks IM, Leck C, Tjernström M (2011) On the potential contribution of open lead particle emissions to the central Arctic aerosol concentration. *Atmos Chem Phys* 11:3093–3105.
37. Draxler RR, Rolph GD (2009) HYSPLIT (Hybrid Single-Particle Lagrangian Integrated Trajectory). *NOAA ARL READY*. Available at: http://readyarlnoaagov/HYSPLITphp. Accessed September 21, 2010.
38. Rolph GD (2010) Real-time environmental applications and display system (READY). Available at: http://readyarlnoaagov. Accessed September 21, 2010.
39. Leck C, Nilsson E, Bigg E, Bäcklin L (2001) The atmospheric program on the Arctic Ocean Expedition in the summer of 1996 (AOE-96): A technical overview: Outline of experimental approach, instruments, scientific objectives. *J Geophys Res Atmospheres* 106:32051–32067.
40. O'Connor EJ, et al. (2010) A method for estimating the turbulent kinetic energy dissipation rate from a vertically pointing doppler lidar, and independent evaluation from balloon-borne in situ measurements. *J Atmos Ocean Technol* 27:1652–1664.
41. Leck C, Bigg EK (2008) Comparison of sources and nature of the tropical aerosol with the summer high Arctic aerosol. *Tellus* 60B:118–126.
42. Orsini D, et al. (2003) Refinements to the particle-into-liquid sampler (Pils) for ground and airborne measurements of water soluble aerosol composition. *Atmos Environ* 37: 1243–1259.
43. Heintzenberg J, et al. (2006) Aerosol number-size distributions during clear and fog periods in the summer high Arctic: 1991, 1996 and 2001. *Tellus* 58B:41–50.
44. Berner A, et al. (1988) The liquid water content of a radiation fog measured by an FSSP 100 optical probe and a fog impactor. *Sci Total Environ* 77:133–140.
45. Ding Y-X, Chin W-C, Verdugo P (2007) Development of a fluorescence quenching assay to measure the fraction of organic carbon present in self-assembled gels in seawater. *Mar Chem* 106:456–462.
46. Dickson AG, Sabine CL, Christian JRE (2007) *Guide to best practices for ocean CO_2 measurements* [North Pacific Marine Science Organization (PICES), Sidney, British Columbia].
47. Bigg E, Leck C (2001) Properties of the aerosol over the central Arctic Ocean. *J Geophys Res Atmospheres* 106:32101–32109.
48. Clayton JJ, Dortch Q, Thoresen S, Ahmed S (1988) Evaluation of methods for the separation and analysis of proteins and free amino acids in phytoplankton samples. *J Plankton Res* 10:341–358.
49. Mopper K, Dawson R (1986) Determination of amino acids in seawater - Recent chromatographic developments and future directions. *Sci Total Environ* 49:115–131.
50. Orellana MV, et al. (2003) Tracing the source and fate of biopolymers in seawater: application of an immunological technique. *Mar Chem* 83:89–99.
51. Keil R, Kirchman D (1991) Dissolved combined aminoacids in marine waters as determined by a vapor-phase hydrolysis method. *Mar Chem* 33:243–259.
52. Hung C-C, et al. (2003) Distributions of carbohydrate species in the Gulf of Mexico. *Mar Chem* 81:119–135.
53. Hung C-C, Tang D, Warnken K, Santschi PH (2001) Distributions of carbohydrates, including uronic acids, in estuarine waters of Galveston Bay. *Mar Chem* 73:305–318.
54. Matrai PA, Keller MD (1993) Dimethylsulfide in a large-scale coccolithophore bloom in the Gulf of Maine. *Cont Shelf Res* 13:831–843.
55. Greenspan P, Fowler SD (1985) Spectrofluorometric studies of the lipid probe, nile red. *J Lipid Res* 26:781–789.
56. Dortch Q, Clayton JRJ, Thoresen SS, Ahmed SI (1984) Species differences in accumulation of nitrogen pools in phytoplankton. *Mar Biol* 81:237–250.
57. Knap A, et al. (1996) Protocols for the Joint Global Ocean Flux Study (JGOFS) Core Measurements. JGOFS Report no. 19, vi+170. *IOC Manuals and Guides* no. 29 (UNESCO, Paris).